Available online at www.sciencedirect.com
ScienceDirect
International Journal of Heat and Mass Transfer 50 (2007) 2148–2160
International Journal of HEAT and MASS TRANSFER
www.elsevier.com/locate/ijhmt

Onset of thermosolutal convection in a shallow porous layer heated and salted from below and subject to a horizontal heat flux balanced by a Soret mass flux

A. Mansour [a], A. Amahmid [a,*], M. Hasnaoui [a], M. Mamou [b]

[a] University Cadi Ayyad, Faculty of Sciences Semlalia, Department of Physics, UFR TMF, BP 2390 Marrakesh, Morocco
[b] Institute for Aerospace Research, National Research Council, Ottawa, Ont., Canada K1A 0R6

Received 13 April 2006; received in revised form 5 November 2006
Available online 11 January 2007

Abstract

In the present paper, a thorough analytical and numerical investigation is carried out to examine the double-diffusive convective instability within a horizontal porous layer heated and salted from below. A situation is considered where a lateral perturbing heat flux applied to the system is balanced by the horizontally induced Soret mass flux. The parameters governing this problem are the thermal Rayleigh number, R_T; the Lewis Number, Le; the buoyancy ratio, N; the Soret parameter, M; the ratio of the horizontal to vertical heat flux, a; and the aspect ratio, A_r; of the porous layer. The present investigation is focused on the situation where $MN = 1$, which describes an equilibrium state between the induced Soret mass flux and the imposed heat flux. For this situation, a rest state solution is possible. The analytical solution, derived on the basis of the parallel flow approximation, is validated numerically using a finite difference method by solving the full governing equations. In the M^*–Le plane ($M^* = 1/M$), five distinct regions, describing different flow behaviors, are delineated and their location depends on the lateral heat flux parameter a. It is also demonstrated that supercritical and/or subcritical bifurcations are possible for specific ranges of M^* and Le. The effect of the lateral heating and the Soret parameter on the critical Rayleigh number, corresponding to the onset of parallel flow convection, is examined. The parameter a affects the flow and the heat transfer considerably, but its effect on the mass transfer is negligible.

Keywords: Numerical and analytical study; Porous media; Thermosolutal convection; Multiplicity of solutions; Soret effect

1. Introduction

The problem of thermo-diffusion, also known as the Soret effect, has received growing attention as it is encountered in nature and in many industrial applications including geophysics, oil reservoirs, multi-component melts and storage of nuclear waste. Theoretical studies on the Soret effect have shown that this phenomenon may engender specific behaviors in convective motions such as multiple steady/oscillatory states, subcritical flows, hysteresis behaviors, Hopf bifurcations and reversal gradients of concentration. A literature review showed that theoretical and experimental efforts have been devoted to understand these phenomena and also to the measurement of the Soret coefficient [1], which is usually unknown and depends on various flow mixture properties.

Rosanne et al. [2] experimentally studied thermo-diffusion in a solution of sodium chloride contained in compact clay. They concluded that the mass transfer was enhanced by the thermal diffusion. Mansour et al. [3] investigated the Soret effect on double-diffusive multiple solutions in a square porous cavity subject to temperature and concentration cross-gradients. Depending on the value and sign of the parameter characterizing the Soret effect, the solute

* Corresponding author. Tel.: +1 212 24 43 46 49x489; fax: +1 212 24 43 74 10.
E-mail address: amahmid@ucam.ac.ma (A. Amahmid).

0017-9310/$ - see front matter © 2006 Elsevier Ltd. All rights reserved.
doi:10.1016/j.ijheatmasstransfer.2006.11.013

Nomenclature

A_r	aspect ratio ($= L'/H'$)
CCF	counter-clockwise flow
CF	clockwise flow
D	mass diffusivity
D^*	thermo-diffusion coefficient
g	gravitational acceleration
H'	height of the porous cavity
j'	constant mass flux per unit area
K	permeability of the porous medium
L'	length of the porous cavity
Le	Lewis number ($Le = \alpha/D$)
M	parameter characterizing the Soret effect ($M = D^* S'_0 \Delta T'/D\Delta S'$)
N	buoyancy ratio ($N = \beta_S \Delta S'/\beta_T \Delta T'$)
Nu	Nusselt number
q'	constant heat flux per unit area
R_T	thermal Darcy–Rayleigh number ($R_T = g\beta_T K q' H'^2/(\lambda\alpha\nu)$)
R_{TC}	critical thermal Rayleigh number
S	dimensionless solute concentration [$S = (S' - S'_0)/\Delta S'$]
S'_0	dimensional solute concentration at the cavity center
$\Delta S'$	concentration solute difference ($\Delta S' = j'H'/D$)
Sh	Sherwood number
T	dimensionless temperature ($T = (T' - T'_0)/\Delta T'$)
t	dimensionless time ($t = t'\alpha/\sigma H'^2$)
T'_0	dimensional temperature at the cavity center
$\Delta T'$	temperature difference ($\Delta T' = q'H'/\lambda$)
u	dimensionless horizontal velocity ($u = u'H'/\alpha$)
v	dimensionless vertical velocity ($v = v'H'/\alpha$)
x	dimensionless distance along the x-axis ($x = x'/H'$)
y	dimensionless distance along the y-axis ($y = y'/H'$)

Greek symbols

α	thermal diffusivity ($\alpha = \lambda/(\rho C)_f$)
β_S	solutal expansion coefficient
β_T	thermal expansion coefficient
ε	normalized porosity ($\varepsilon = \varepsilon'/\sigma$)
ε'	porosity of the porous medium
λ	thermal conductivity of the saturated porous medium
ν	kinematic viscosity of the fluid
ρ	density of the fluid mixture
$(\rho c)_f$	heat capacity of fluid mixture
$(\rho c)_p$	heat capacity of the saturated porous medium
σ	heat capacity ratio ($\sigma = (\rho c)_p/(\rho c)_f$))
Ψ	dimensionless stream function ($\Psi = \Psi'/\alpha$)

Superscript

$'$	dimensional variables

could be transferred from the least to the most salted wall, leading to negative values of the Sherwood number. The choice of this parameter was found to affect the presence of the multicellular flow in the enclosure. The problem of thermo-diffusion in an initially homogeneous mixture submitted to a horizontal thermal gradient was studied numerically and experimentally by Benano et al. [4]. Their numerical results showed that multiple convection-roll flow patterns could develop in the presence of counter-acting thermal and solutal buoyancy forces, depending on the Soret number value. The discrepancy observed between the numerical and experimental results was attributed to the dispersion effect. Thermosolutal natural convection induced in a binary mixture and confined in a slightly inclined tall enclosure was investigated analytically and numerically by Ouriemi et al. [5] in the presence and absence of the Soret effect. The cavity was heated from below with a constant heat flux and its long side walls were impermeable and adiabatic. The existence of multiple steady states was demonstrated for sufficiently small inclinations around the vertical plane. The Soret effect on convection in a horizontal porous cavity submitted to cross gradients of temperature and concentration was considered by Bennacer et al. [6]. Their results showed that when the vertical concentration gradient was stabilizing, multiple steady-state solutions were possible over a range of buoyancy ratios that depended strongly on the Soret parameter. Among the problems studied recently in the thermo-diffusion field were those related to the Soret effect on the onset of convection flows in rectangular porous enclosures. The investigation conducted by Marcoux et al. [7] was devoted to study the onset of thermogravitational diffusion within a vertical porous cavity subject to horizontal thermal gradients in the case of opposing and equal thermal and solutal buoyancy forces. A linear stability analysis of the purely diffusive state was performed and the thresholds of instability were computed for various enclosure aspect ratios. Their numerical results showed different flow structures and the existence of time-periodic oscillatory solutions. The onset of natural convection within a vertical porous layer subject to uniform heat fluxes along the vertical walls was also studied analytically and numerically by Joly et al. [8] using the Brinkman–extended Darcy model. The Soret effect in this problem was such that the solutal and thermal buoyancy forces had opposing effects and were of the same order of magnitude. Both supercritical and subcritical bifurcations were possible in the system. Rehberg and Ahlers [9] studied experimentally bifurcations phenomena in a horizontal porous layer of a normal-fluid ^{3}He–^{4}He mixture heated from below. Their study showed that the

nature of bifurcation from the rest state depended on the separation ratio and hysteresis phenomena were possible for this problem. The effect of the gravity gradient on the onset of thermosolutal convection due to thermal diffusion in a fluid saturated isotropic porous layer with horizontal boundaries maintained at constant but different temperatures and concentrations was studied by Alex and Patil [10]. The authors showed that the Soret parameter affected the pattern of convection only when its magnitude was large in the presence and absence of the gravity field variations. The onset of Soret-driven convection in an infinite porous layer saturated by a binary fluid with impermeable horizontal walls maintained at different and uniform temperatures was investigated by Sovran et al. [11]. The criteria for the onset of motion via a stationary and Hopf bifurcations were determined using a linear stability analysis. They showed that the bifurcation from the rest state depended, among other factors, on the separation ratio. Bénard convection in a porous layer filled with a binary liquid exhibiting a nonlinear density–temperature relation was investigated by Karcher and Müller [12] in the presence of the Soret effect. They found that non-Boussinesq properties have a destabilizing effect on the rest state regime. The Soret effect on thermosolutal convection within a shallow horizontal porous layer subject to a vertical uniform heat flux was investigated analytically and numerically by Bahloul et al. [13]. The thresholds for finite-amplitude, oscillatory and monotonic convection instabilities were determined in terms of the governing parameters using linear and nonlinear stability analyses. The existence of subcritical convection was predicted for negative values of the Soret parameter. A similar problem was studied by Bourich et al. [14] by performing a comparative study for the limiting cases, which considered Darcy porous and clear fluid media. A closed form analytical solution for a shallow enclosure was derived on the basis of the parallel flow approximation and the onset of overstabilities was predicted using a linear stability analysis. An appropriate normalization for the Rayleigh number was used to demonstrate that the flow behavior was similar to that predicted by the parallel flow assumption for any aspect ratio of the enclosure. The same authors [15] analytically and numerically investigated the Soret effect on thermosolutal convection induced in a horizontal Darcy porous layer subject to constant heat and mass fluxes. The thresholds for the onset of supercritical and subcritical convection were predicted explicitly as functions of the governing parameters. They demonstrated that there existed combinations of the governing parameters for which the Soret effect imposed a vertical non-linear stratification of the concentration field, even for a convective regime, and that a reversal horizontal concentration gradient was also possible. Ryskin et al. [16] studied the Soret effect on thermo-convection in a horizontal infinite layer of binary liquid mixtures with weak concentration diffusivity and large separation numbers. By considering the classical Rayleigh Bénard problem, they showed that both linear and nonlinear convective behaviors were significantly altered by the concentration field as compared to single-component systems. Delahaye et al. [17] analytically and numerically investigated the Soret effect on convection in a horizontal fluid layer with a free upper surface. The layer was heated from below, cooled from above, and all its boundaries were impermeable to mass transfer. The critical Rayleigh numbers for the onset of supercritical and subcritical convection were predicted in terms of the governing parameters of the problem. The effect of a shear stress applied on the free upper boundary of a horizontal fluid layer of a binary mixture with a Soret contribution was studied both analytically and numerically by Mahidjiba et al. [18]. The boundaries of the system were impermeable to mass transfer and subjected to uniform heat fluxes. The occurrence of multiple steady-state solutions was demonstrated for given sets of the control parameters. Ouriemi et al. [19] studied analytically and numerically thermo-diffusion in an inclined shallow cavity filled with a binary fluid. Newmann boundary conditions for temperature are applied to the long side walls of the enclosure, while the two short ones are assumed to be impermeable and insulated. Supercritical and subcritical convection is predicted in the case of a horizontal layer. The existence of "natural" and "antinatural" flows is also demonstrated by these authors for $\varphi > 0$. Charrier-Mojtabi et al. [20] investigated thermosolutal natural convection with Soret effect under the simultaneous action of vibrational and gravitational accelerations in a porous cavity saturated by a binary mixture. The problem was examined for different aspect ratios with various directions of vibration. It is concluded that, for both the stationary and the Hopf bifurcations, the vertical vibration has a stabilizing effect while the horizontal vibration has a destabilizing effect on the onset of convection.

The object of the present paper consists of predicting the onset of double-diffusive natural convection flows developed in a horizontal porous layer subject to uniform fluxes of heat and mass on its long sides. Attention is focused on the situation where the lateral imposed heating flux is balanced by the horizontally induced Soret mass flux which leads to an equilibrium state (motionless state) that becomes unstable under certain conditions. To examine the induced flow behavior, finite amplitude solutions of the full governing equations were obtained analytically, using the parallel flow approach, and numerically using a finite difference method. The present thermo-diffusion problem is found to exhibit a rich variety of different bifurcation phenomena.

2. Mathematical formulation

The configuration considered in this study, sketched in Fig. 1, is a two-dimensional horizontal porous layer of length L' and height H'. The origin of the coordinate system (x' is the horizontal axis and y' is the vertical axis opposing gravity) is taken at the geometric center of the cavity. The long horizontal walls of the cavity are subject to uniform

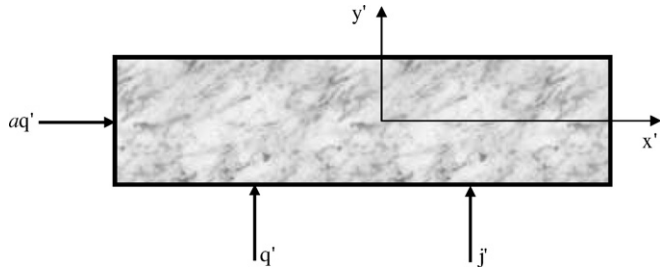

Fig. 1. Schematic diagram of the studied configuration.

fluxes of heat, q', and mass j', while its short walls are impermeable to mass transfer and exposed to a constant heat flux of intensity aq'. The porous medium is homogeneous and isotropic and the inertia effects are neglected by assuming low Reynolds flows. The binary solution that saturates the porous medium is modeled as a Boussinesq incompressible fluid whose density varies linearly with the temperature and concentration ($\rho = \rho_0[1 - \beta_T(T' - T'_0) - \beta_S(S' - S'_0)]$). The variations of the latter in the medium are assumed small enough for the other physical properties to remain constant.

Using the Darcy model and taking into account the Soret effect, the governing equations are written as follows:

$$\nabla^2 \Psi = -R_T\left(\frac{\partial T}{\partial x} + N\frac{\partial S}{\partial x}\right) \tag{1}$$

$$\nabla^2 T = \frac{\partial T}{\partial t} + \frac{\partial (uT)}{\partial x} + \frac{\partial (vT)}{\partial y} \tag{2}$$

$$\frac{1}{Le}(\nabla^2 S + M\nabla^2 T) = \varepsilon\frac{\partial S}{\partial t} + \frac{\partial (uS)}{\partial x} + \frac{\partial (vS)}{\partial y} \tag{3}$$

$$u = \frac{\partial \Psi}{\partial y}, \quad v = -\frac{\partial \Psi}{\partial x} \tag{4}$$

where Ψ, T and S are the dimensionless stream function, temperature and solute concentration, respectively. The boundary conditions associated to the problem are

$$\Psi = 0, \quad \frac{\partial T}{\partial x} = -a; \quad \frac{\partial S}{\partial x} = aM, \quad \text{for } x = \pm\frac{A_r}{2} \tag{5}$$

$$\Psi = 0, \quad \frac{\partial T}{\partial y} = -1; \quad \frac{\partial S}{\partial y} = -1 + M, \quad \text{for } y = \pm\frac{1}{2} \tag{6}$$

The above equations show that the steady state solutions of the present problem are governed by six dimensionless parameters, namely, the thermal Rayleigh number, R_T; the buoyancy ratio, N; the Lewis number, Le; the Soret parameter, M; the ratio of horizontal to vertical heat fluxes, a; and the enclosure aspect ratio, A_r. They are defined as follows:

$$R_T = \frac{g\beta_T K\Delta T' H'}{\alpha\nu}, \quad Le = \frac{\alpha}{D}, \quad N = \frac{\beta_S \Delta S'}{\beta_T \Delta T'},$$
$$M = \frac{D * S'_i \Delta T'}{D\Delta S'}, \quad A_r = \frac{L'}{H'} \tag{7}$$

The use of the Soret parameter, M, makes it possible to reproduce the results that can be obtained in the absence of the Soret effect by setting $M = 0$. The present normalization is somewhat similar to that used by Alex and Patil [10].

The heat and solute transfer rates across the layer are characterized by the Nusselt and Sherwood numbers, which are defined as

$$Nu = \frac{1}{[T(0,-1/2) - T(0,1/2)]} \tag{8}$$

$$Sh = \frac{1}{[S(0,-1/2) - S(0,1/2)]} \tag{9}$$

3. Numerical solution

The numerical solution of the full governing equations was obtained using a second-order finite-difference scheme. The temperature and concentration equations, Eqs. (2) and (3), were solved iteratively using the alternate direction implicit method. Nodal values of the stream function were obtained from Eq. (1) via a point successive-over-relaxation method. Details concerning the validation of the present code in the absence of the Soret effect were reported in Bourich et al. [21]. The present numerical code was successfully used by Bourich et al. [12,13] in the presence of the Soret effect, and it was validated by comparing the results with an exact analytical solution developed for a horizontal porous layer of infinite extent. A grid size of 301×61 was used for the range of the governing parameters considered in the present study. This grid size produces good agreement between the numerical and analytical results. A non uniform grid was used in the horizontal direction for large aspect ratio enclosures to capture the flow details in the end regions.

4. Analytical solution

The analytical solution was developed for steady-state flows using a parallel flow approximation, which leads to the following simplifications:

$$\Psi(x,y) = \Psi(y), \quad T(x,y) = C_T x + \theta_T(y), \quad \text{and}$$
$$S(x,y) = C_S x + \theta_S(y)$$

where C_T and C_S are unknown constant temperature and solute concentration gradients, respectively, in the horizontal direction. Using the above approximations, the governing Eqs. (1)–(3) may be reduced to the following ordinary differential equations:

$$\frac{d^2\Psi}{dy^2} = -R_T(C_T + NC_S) \tag{10}$$

$$\frac{d^2\theta_T}{dy^2} = C_T\frac{d\Psi}{dy} \tag{11}$$

$$\frac{d^2\theta_S}{dy^2} = LeC_S\frac{d\Psi}{dy} \tag{12}$$

The boundary conditions on the horizontal walls $\left(y = \pm\frac{1}{2}\right)$ become

$$\Psi = 0, \quad \frac{\partial\theta_T}{\partial y} = -1 \quad \text{and} \quad \frac{\partial\theta_S}{\partial y} = -1 + M \tag{13}$$

The constants C_T and C_S were determined by performing a global balance of energy and solute transfer across any transversal section of the layer (Trevisan and Bejan [22]). These balances lead to the following integrals:

$$\int_{-\frac{1}{2}}^{\frac{1}{2}} \left(uT - \frac{\partial T}{\partial x}\right) dy = a \tag{14}$$

$$\int_{-\frac{1}{2}}^{\frac{1}{2}} \left[uS - \frac{1}{Le}\left(\frac{\partial S}{\partial x} + M\frac{\partial T}{\partial x}\right)\right] dy = 0 \tag{15}$$

The solutions of Eqs. (10)–(12), satisfying conditions (13) were obtained as follows:

$$\Psi(y) = \Psi_0(1 - 4y^2) \tag{16}$$

$$T(x,y) = C_T x - y - 4\Psi_0 C_T\left(\frac{y^3}{3} - \frac{y}{4}\right) \tag{17}$$

$$S(x,y) = C_S x + (M-1)y - 4\Psi_0(LeC_S + C_T)\left(\frac{y^3}{3} - \frac{y}{4}\right) \tag{18}$$

where Ψ_0 is the value of the stream function at the center of the porous layer defined by

$$\Psi_0 = \frac{R_T}{8}(C_T + NC_S) \tag{19}$$

Substituting Eqs. (17) and (18) into Eqs. (8) and (9), the analytical expressions of Nusselt and Sherwood numbers may be given by

$$Nu = \frac{3}{3 - 2C_T\Psi_0} \tag{20}$$

$$Sh = -\frac{3}{3(M-1) + 2\Psi_0(LeC_S - MC_T)} \tag{21}$$

where

$$C_T = \frac{-5(3a - 2\Psi_0)}{15 + 8\Psi_0^2} \tag{22}$$

$$C_S = \frac{-10Le\Psi_0(M-1) + MC_T(8Le\Psi_0^2 - 15)}{15 + 8Le^2\Psi_0^2} \tag{23}$$

Substituting Eqs. (22) and (23) into Eq. (19) yields the following equation for Ψ_0:

$$\Psi_0^5 + A\Psi_0^3 + B\Psi_0^2 + C\Psi_0 + D = 0 \tag{24}$$

with

$$\begin{cases} A = 80d[12(Le^2+1) - R_T Le(N+Le)], \\ B = 120daR_T Le(Le - \varphi), \\ C = -150dR_T[(NLe+1) + \varphi(Le+1)] + 1800d, \\ D = 225daR_T(1+\varphi) \end{cases}$$

where $d = \frac{1}{512Le^2}$ and $\varphi = -MN$.

For given values of R_T, Le, M, N and a, the above transcendental equation can be solved analytically, or numerically using a Newton–Raphson technique. The present study focuses on a special case for which the rest state ($\Psi_0 = 0$) is a possible solution for the governing Eqs. (1)–(4). From the latter, it can be demonstrated that the rest state is possible if and only if $MN = 1$, or when the effect of the imposed heat flux on the vertical boundaries is entirely balanced by the induced Soret mass flux. This equilibrium state cannot be realized in the absence of the Soret effect (i.e., $M = 0$). For this particular case, the parameter D of Eq. (24) becomes null. The four solutions of Eq. (24), for finite amplitude convection, are obtained analytically as follows:

$$\Psi_0 = \frac{-A_1 \pm \sqrt{D_1}}{2} \quad \text{for } D_1 \geqslant 0 \quad \text{and}$$

$$\Psi_0 = \frac{A_1 \pm \sqrt{D_2}}{2} \quad \text{for } D_2 \geqslant 0$$

where $D_1 = A_1^2 - 4B_1$ and $D_2 = A_1^2 - 4C_1$. The other constants are

$$A_1 = \sqrt{E - A}, \quad B_1 = \frac{1}{2}\left(A + A_1^2 - \frac{B}{A_1}\right) \quad \text{and}$$

$$C_1 = \frac{1}{2}\left(A + A_1^2 + \frac{B}{A_1}\right),$$

$$E = \frac{U_1}{|U_1|}(|U_1|)^{\frac{1}{3}} + \frac{V_1}{|V_1|}(|V_1|)^{\frac{1}{3}} - \frac{a'}{3} \quad \text{if } \Delta > 0$$

and

$$E = \text{Max}(E_1, E_2, E_3) \quad \text{if } \Delta \leqslant 0$$

where

$$U_1 = -\frac{q}{2} + \sqrt{\Delta}, \quad V_1 = -\frac{q}{2} - \sqrt{\Delta},$$

$$\Delta = \left(\frac{p}{3}\right)^3 + \left(\frac{q}{2}\right)^2, \quad p = b - \frac{a'^2}{3},$$

$$q = \frac{2}{27}a'^3 - \frac{a'b}{3} + c, \quad a' = -A,$$

$$b = -4C, \quad c = 4AC - B^2,$$

$$E_1 = 2\sqrt{\frac{-p}{3}}\cos\left(\frac{\theta_0}{3}\right) - \frac{a'}{3},$$

$$E_2 = 2\sqrt{\frac{-p}{3}}\cos\left(\frac{\theta_0 + 2\pi}{3}\right) - \frac{a'}{3},$$

$$E_3 = 2\sqrt{\frac{-p}{3}}\cos\left(\frac{\theta_0 + 4\pi}{3}\right) - \frac{a'}{3}$$

and

$$\theta_0 = \arccos\left(\frac{3q}{2p}\sqrt{\frac{-3}{p}}\right)$$

Recall that, in the absence of mass transfer, lateral heating makes the system unconditionally unstable and convection exists for any $R_T > 0$. In the forgoing analysis, the

buoyancy ratio N is substituted by $M^* = M^{-1}$, and the problem becomes governed by four parameters, which are R_T, Le, M^* and a.

5. Results and discussion

For a shallow enclosure, the parallel flow solution given by Eq. (24) shows that a supercritical bifurcation occurs at Rayleigh number given by

$$R_{TC}^{sup} = \frac{12}{Le(M^* - 1)}$$

The expression of R_{TC}^{sup} shows that this bifurcation is possible only for $0 < M < 1$. The mathematical solution of Eq. (24) also shows that two types of subcritical bifurcations are possible. The first one occurs at R_{TC}^{sub1} ($D_1 \geqslant 0$), while the second one, when it exists, appears at R_{TC}^{sub2} ($D_2 \geqslant 0$). Note that supercritical bifurcation is always preceded by one subcritical bifurcation. In the absence of the lateral heating, it has been demonstrated [15] that there are situations where only supercritical convection is possible. The variations of R_{TC}^{sub1}, R_{TC}^{sub2} and R_{TC}^{sup} with M^* are presented in Fig. 2 for $Le = 7$ and $a = 0.5$. This figure shows that supercritical and subcritical bifurcations are possible for $M^* > 1$ (with $R_{TC}^{sup} > R_{TC}^{sub1}$). In the range $1 < M^* \leqslant 1.98$, two subcritical bifurcations and a supercritical one exist, but the latter disappears for $M^* < 1$. In the case of $a \neq 0$, it is to note that the supercritical bifurcation leads to the disappearance of the clockwise unstable flow in favor of the counter-clockwise one (or the inverse) when M^* is varied around the supercritical point (see Fig. 4a). In the range $-7.6 < M^* < -7$, only one subcritical bifurcation persists and no parallel flow solution is possible for $M^* < -7.6$. On the basis of these observations, the M^*–Le plane can be divided into five regions with specific behaviors (Fig. 3a). These regions are separated by curves which depend on the parameter a. Region (I) is defined by $M^* \geqslant M_1 = \lfloor (1 - Le) + (1 + Le)\sqrt{1 + (6/5)a^2} \rfloor / 2$. In this region, when M^* is close to M_1^*, two subcritical bifurcations and a supercritical one are obtained at $R_T = R_{TC}^{sub1}$, R_{TC}^{sub2} and R_{TC}^{sup}, respectively, which leads to four convective solutions over a given range of R_T. However, there exists a threshold of R_T, R_{TC}^{D}, above which two of these solutions disappear. The evolution of R_{TC}^{D} with M^* is illustrated in Fig. 2 where it is seen that it tends towards infinity at some point corresponding to the passage from region (I) to region (II). For values of M^* far from the limit M_1^*, one of the two subcritical bifurcations disappears and two solutions are obtained regardless of R_T. In the second region (II), defined by $M_1^* \geqslant M^* > 1$, two subcritical bifurcations and a supercritical one are obtained, and the corresponding four convective solutions persist for any R_T greater than R_{TC}^{sub2}. For the third region (III), corresponding to $1 > M^* \geqslant -Le$, two subcritical bifurcations (leading to four solutions) persist, but the supercritical one disappears. In the fourth

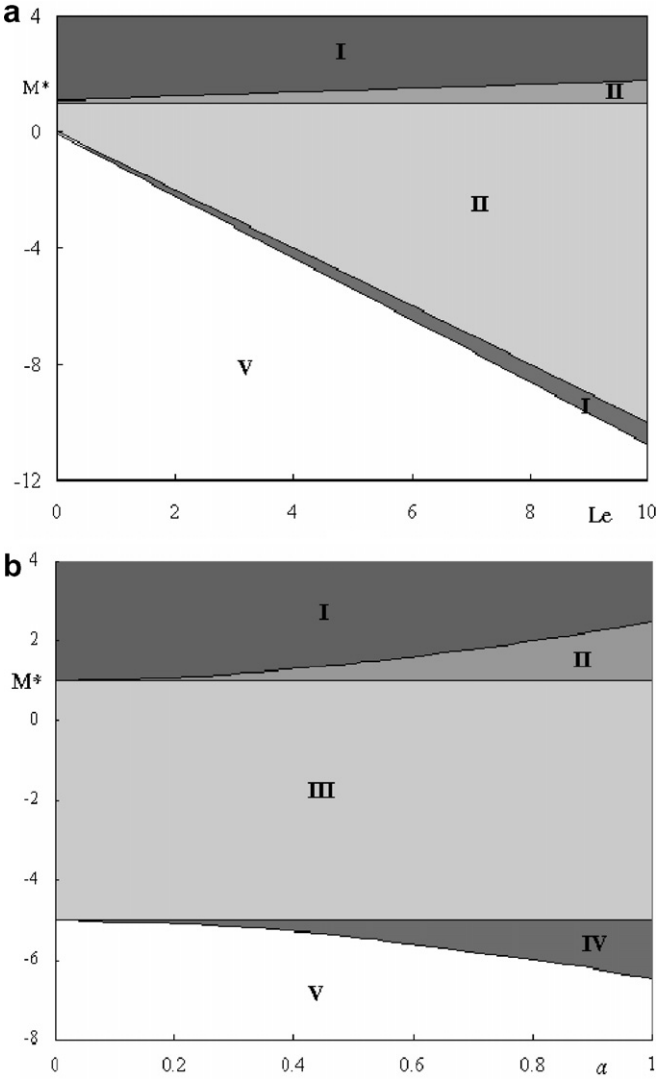

Fig. 3. Regions corresponding to different modes of convection for $R_T = 50$ in the plane (a) (Le–M^*) for $a = 0.5$ and (b) (Le–a) for $Le = 5$.

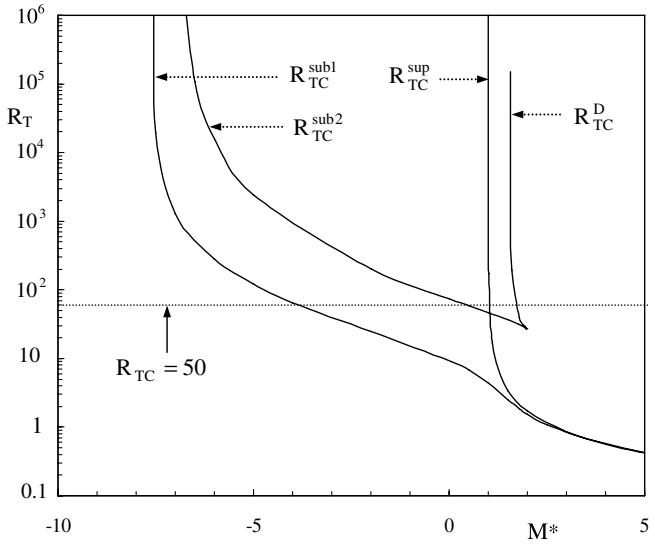

Fig. 2. Stability diagram of R_T versus M^* for $Le = 7$ and $a = 0.5$.

region (IV), defined by $-Le > M^* \geqslant \lfloor(1-Le)-(1+Le)\sqrt{1+(6/5)a^2}\rfloor/2$, only one subcritical bifurcation (two convective solutions) exists. Finally, in the last region (V), defined by $M^* < \lfloor(1-Le)-(1+Le)\sqrt{1+(6/5)a^2}\rfloor/2$, the parallel flow solution does not exist, regardless of R_T. These regions are also presented in the M^*–a plane for $Le = 5$, as shown in Fig. 3b. For the latter case, the thickness of the third region is independent of the parameter a when Le is fixed.

The effect of M^* on the fluid flow and heat and mass transfer characteristics is illustrated in Fig. 4a–c for $R_T = 50, Le = 7$ and $a = 0$ (absence of the lateral heating) and 0.5. The curve of Ψ_0, presented in Fig. 4a, exhibits a symmetrical behavior for $a = 0$, with two subcritical bifurcations starting at the same value of $M^* = -1.314$. This symmetry is destroyed in the presence of lateral heating, leading to imperfection bifurcation. As a consequence, one of the two subcritical bifurcations is retarded (occurs at $M^* \approx 0.87$) and the other one starts earlier (occurs at $M^* \approx -3.5$). These values of M^* can also be deduced from Fig. 2 as intersection points between the line $R_T = 50$ and the bifurcation curves. Fig. 4a displays also the onset point for subcritical convection beyond which the rest state solution $\Psi_0 = 0$ becomes unstable to finite amplitude perturbations and the onset point for supercritical convection beyond which the rest state is unstable to infinitesimal perturbations. The dashed lines are used for the unstable branches of the curves; which could not be obtained numerically. By increasing M^* from -3.5, the dashed branch crosses the line $\Psi_0 = 0$ at the point $M^* \cong 1$ where the supercritical bifurcation starts. At sufficiently large M^*, only the two stable branches persist. Fig. 4a also indicates that there is a range of M^* over which four parallel flow solutions are possible. The effect of M^* on Nu, presented in Fig. 4b, indicates that Nu is considerably reduced by the flow rotating in the counter-clockwise direction. This flow tends to transport heat from the lateral heated wall towards the bottom heated wall. The variations of Sh with M^*, presented in Fig. 4c, are characterized by a special behavior. For a given value of M^*, all the obtained solutions lead almost to the same Sh. Furthermore, there is a value of M^* for which Sh tends towards infinity, indicating that the concentration difference between the top and bottom walls of the porous layer is zero for a given vertical section. This behavior was inspected more closely through the concentration profile obtained in such a situation for $Le = 7, M^* = 0.82, a = 0.5$ and $R_T = 50$ (results not presented). It was found that, globally, the concentration in the lower part of the porous layer is higher than that in the upper part, even though the horizontal boundaries have the same concentration for this case. Also note that the Sh values presented in Fig. 4c can be negative or positive as the thermal diffusion may transport the solute upward or downward depending on the sign of M^*.

The effect of the flow rotation (clockwise and counter-clockwise) on the velocity, temperature and concentration fields, is illustrated in Fig. 5a and b (iso-contours) and

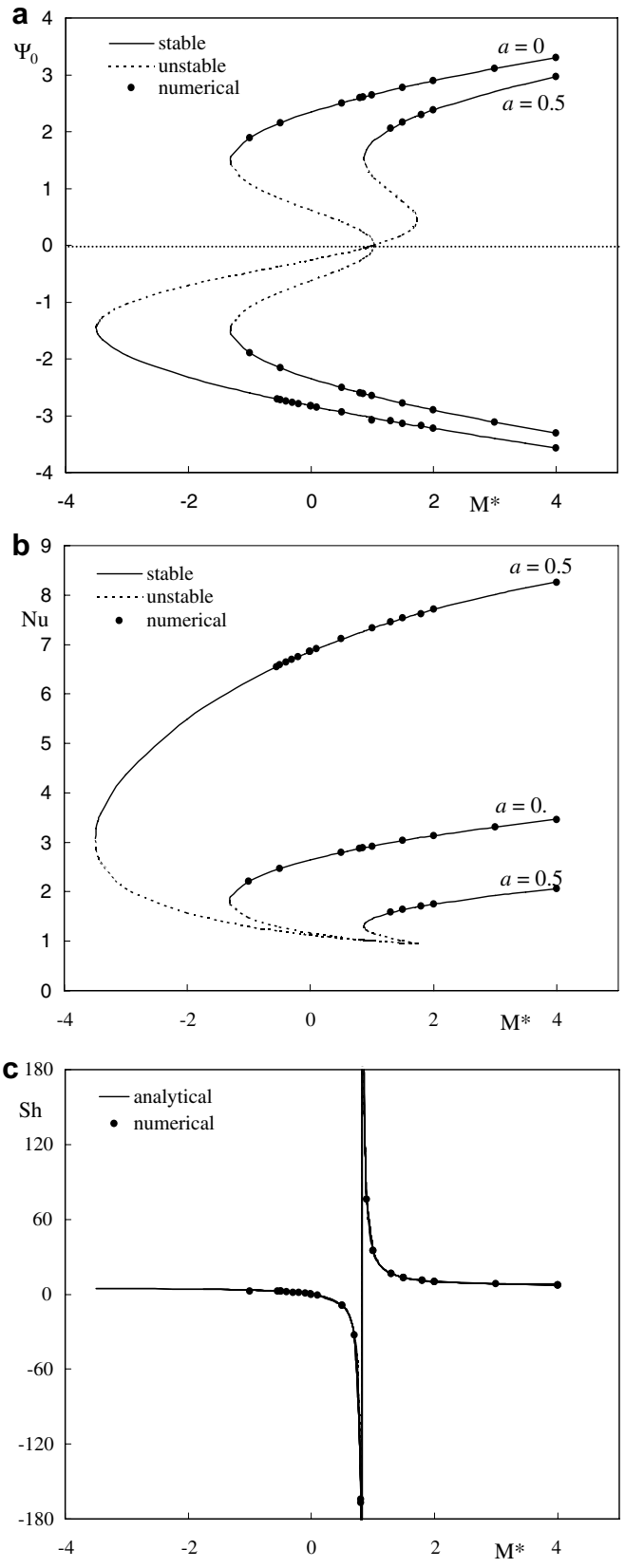

Fig. 4. Effect of M^* on (a) Ψ_0, (b) Nu and (c) Sh for $R_T = 50$, $Le = 7$ and $a = 0$ and 0.5.

Fig. 6a–c (mid-width profiles) for $R_T = 50, Le = 7, a = 0.5$ and $M^* = 3$. These flows correspond to the same set of

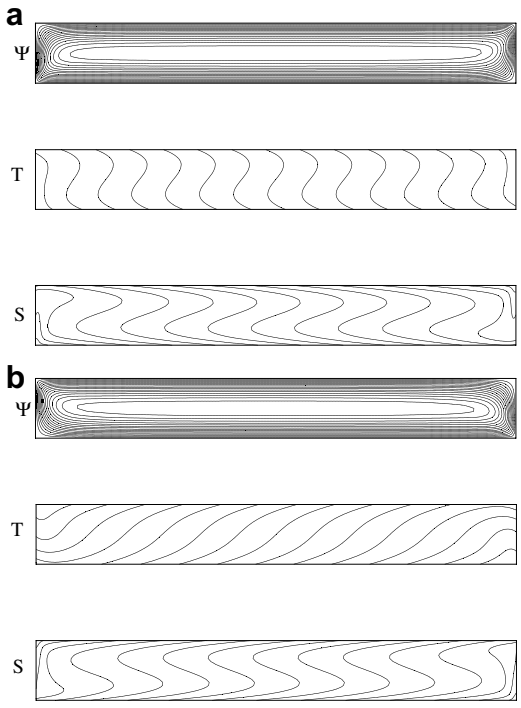

Fig. 5. Typical streamlines and temperature and concentration contours for $A_r = 8$, $R_T = 50$, $Le = 7$, $M^* = 3$ and $a = 0.5$ corresponding to (a) clockwise flow ($\Psi_0 = -3.40335$, $Nu = 8.0225$ and $Sh = 8.30112$) and (b) counter-clockwise flow ($\Psi_0 = 2.7083$, $Nu = 1.92086$ and $Sh = 8.2934$).

governing parameters and the numerical solutions were obtained using the parallel flow solutions as initial conditions. The streamlines of Fig. 5a (CF) and b (CCF) shows clearly that the flow is parallel to the horizontal boundaries for both solutions. The convection effect on the temperature fields is more pronounced in the case of the clockwise solution. However, the concentration fields remain qualitatively similar if we accept that the deformation of the isocontours follows the direction of the flow rotation. The mid-width profiles of temperature, concentration and velocity, presented in Fig. 6a–c, indicate that both flows induce the same profile for concentration but different profiles for temperature and velocity. These figures show also that the analytical solution is well reproduced numerically.

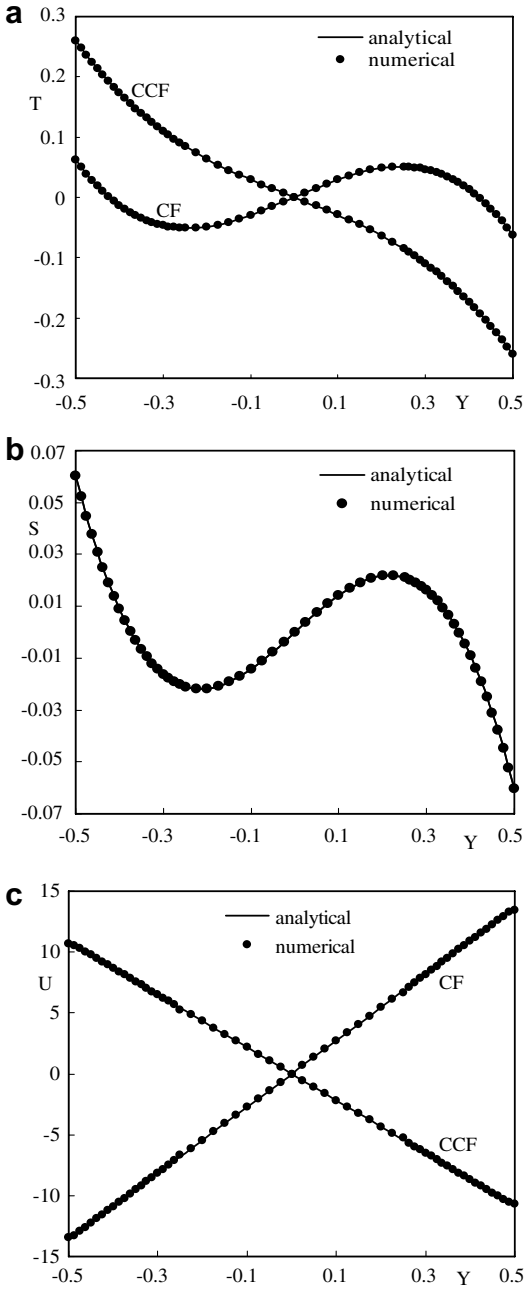

Fig. 6. Vertical profiles at the mid-width of the enclosure for $A_r = 12$, $Le = 7$, $R_T = 50$, $M^* = 3$ and $a = 0.5$: (a) temperature profile, (b) concentration profile and (c) velocity profile.

5.1. Effect of R_T for different regions

The effect of the R_T on the fluid flow and heat and mass transfer characteristics depends on the governing parameters ranges that are described by the different regions shown in Fig. 3. Fig. 7a–c shows the evolution of the flow intensity, Ψ_0; the Nusselt number, Nu; and the Sherwood Number, Sh; with R_T for $a = 0.5$ and various values of (Le, M^*). All the curves presented in these graphs correspond to parallel flow solutions. The numerical solution of the full governing equations is in good agreement with the analytical model. For $(Le, M^*) = (7, 2.5)$, only one subcritical bifurcation appears at $R_{TC}^{sub} = 1.09$, with two solutions engendering clockwise rotating cells. For $R_T > R_{TC}^{sup} = 1.143$, the flow circulation corresponding to one of these two solutions becomes counter-clockwise. The intensity of the latter (i.e. $|\Psi_0|$) decreases slightly between R_{TC}^{sub} and R_{TC}^{sup}. For $(Le, M^*) = (7, 1.5)$, a first subcritical bifurcation manifests at $R_{TC}^{sub1} = 2.5034$, marking the onset of two clockwise flows. By increasing R_T up to $R_{TC}^{sup} = 3.43$, one of these flow solutions becomes counter-clockwise. The intensity of the clockwise flow increases monotonously with R_T while the intensity of the counterclockwise flow presents an asymptotic behavior. The second subcritical bifurcation occurs at $R_{TC}^{sub2} = 36.7$ and induces two solutions characterized by

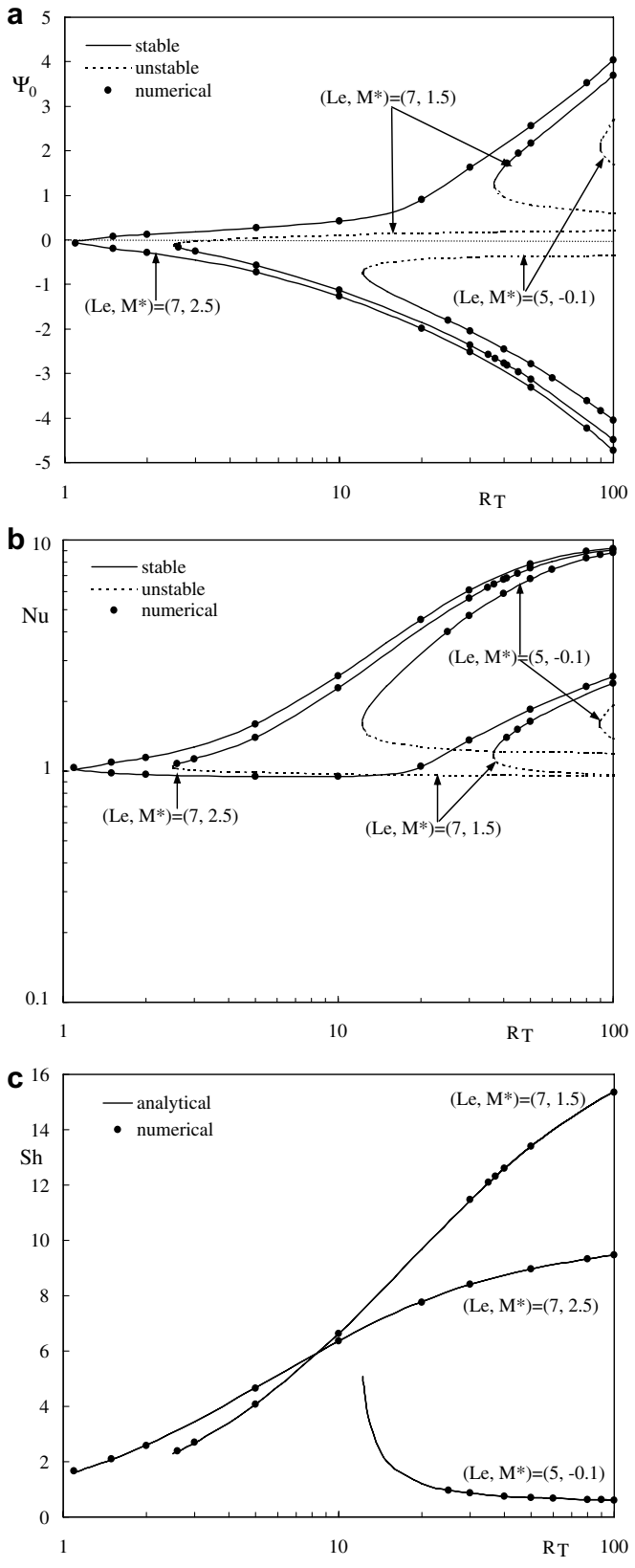

Fig. 7. Effect of R_T on (a) Ψ_0, (b) Nu and (c) Sh, for $a = 0.5$ and different regions.

counter-clockwise flows for any $R_T > R_{TC}^{sub2}$. For the last value $(5, -0.1)$ of (Le, M^*), the behavior is qualitatively similar to that described for $(7, 1.5)$ but without any supercritical bifurcation.

The effect of the convective bifurcation on the Nusselt number is presented in Fig. 7b. For $(Le, M^*) = (7, 2.5)$, characterized by a single subcritical bifurcation, the two obtained solutions lead to different behaviors for the Nusselt number. For the solution where the flow always remains clockwise, Nu increases and reaches a maximum value at $R_T \approx 130$, then decreases towards an asymptotic limit (reached at $R_T > 10^4$). For the solution that changes its flow rotating direction, Nu goes through a minimum at $R_T \approx 5$ and then increases afterwards to an asymptotic limit of the first solution. Two bifurcations are obtained for $(Le, M^*) = (7, 1.5)$. The first one yields two clockwise flows. One of these (continuous line) has a behavior similar to that engendered by the clockwise flow corresponding to $(Le, M^*) = (7, 2.5)$; the other (dashed line) is characterized by a decrease of Nu with R_T. The second bifurcation induces lower Nusselt numbers; however, the stable branches of both solutions lead to the same asymptotic limit. Generally, the Nusselt number induced by the different solutions, corresponding to different regions, has an asymptotic behavior for high values of R_T. Note that there are situations for which $Nu < 1$ ($Nu = 1$ for the rest state). This phenomenon results from the effect of the lateral heating, which heats the fluid coming from the vicinity of the cold wall. Fig. 7c shows the evolution of Sh with R_T for the different obtained solutions. The convective solutions corresponding to a given combination of (Le, M^*, a, R_T) induce nearly the same Sherwood number. The evolution of Sh is characterized by an increase or a decrease with R_T, depending on the combination (Le, M^*), and presents an asymptotic behavior at large R_T (reached at $R_T > 10^3$).

5.2. Effect of the lateral heating on the critical parameters

The influence of the parameter a on the subcritical and supercritical Rayleigh numbers and on the critical value of Ψ_0 (Ψ_{0cr} denotes the flow intensity at the onset of the subcritical convection) is illustrated in Fig. 8a and b and 9a and b for $(Le, M^*) = (3, 2)$ and (1.5, 1.5), respectively. For the combination $(Le, M^*) = (3, 2)$, where one subcritical and one supercritical bifurcations are obtained, Fig. 8a shows that R_{TC}^{sup} is independent of the lateral heating in accordance with the relation $R_{TC}^{sup} = 12/[Le(M^* - 1)]$. An increase of a induces a reduction of R_{TC}^{sub}, which leads to a rest state that is more and more unstable. Note that for $a = 0$, $R_{TC}^{sub} = R_{TC}^{sup} = 4$ for this case; this behavior is characteristic of a region where only one subcritical bifurcation exists. Fig. 8b indicates a monotonic increase of $|\Psi_{0cr}|$ with a. Quantitatively, $|\Psi_{0cr}|$ passes from 0 to 0.28 when the value of a increases from 0 to 1. For the combination $(Le, N) = (1.5, 1.5)$, for which two subcritical bifurcations and a supercritical one exist, Fig. 9a and b shows the effect of a on R_{TC}^{sup}, R_{TC}^{sub1}, R_{TC}^{sub2}, $|\Psi_{0cr}^1|$ ($\Psi_{0cr}^1 = \Psi_{0cr}$ at the onset of the clockwise flow) and Ψ_{0cr}^2 ($\Psi_{0cr}^2 = \Psi_{0cr}$ at the onset of the counter-clockwise flow). The obtained values of the stream

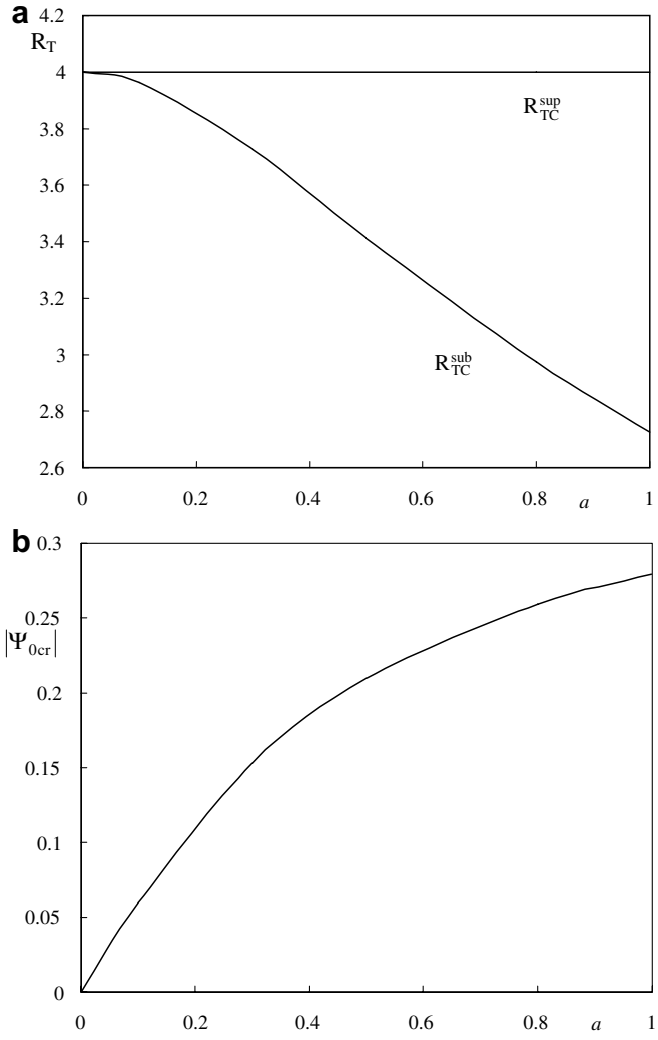

Fig. 8. Effect of a on (a) R_{TC}^{sup} and R_{TC}^{sub} and (b) $|\Psi_{0cr}|$ for $Le = 3$ and $M^* = 2$.

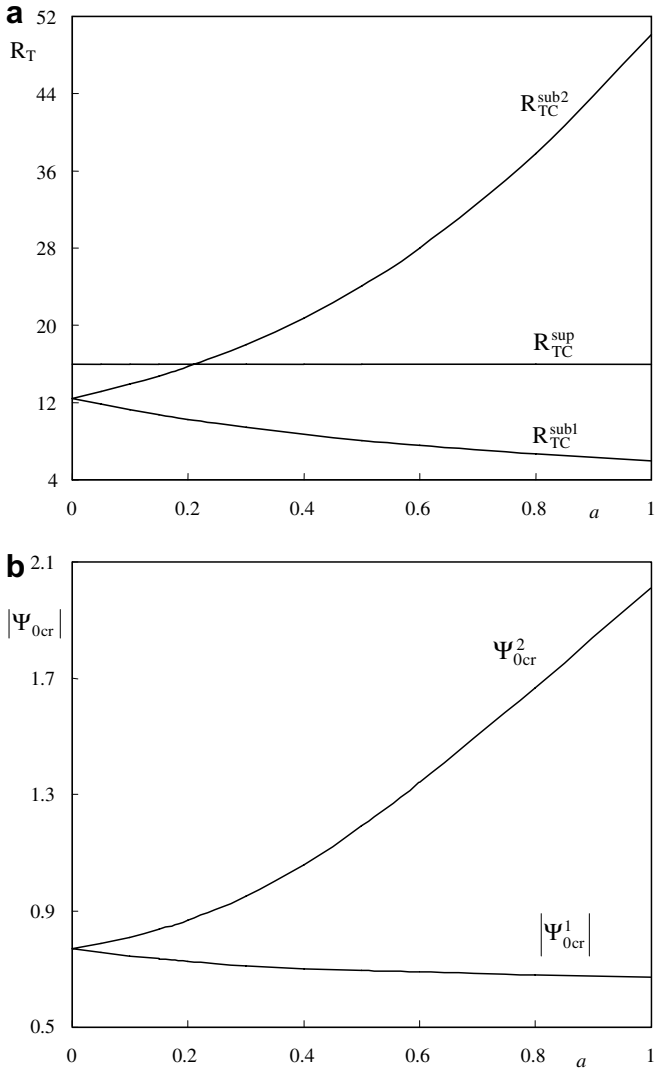

Fig. 9. Effect of a on (a) R_{TC}^{sup}, R_{TC}^{sub1} and R_{TC}^{sub2} and (b) $|\Psi_{0cr}^1|$ and $|\Psi_{0cr}^2|$ for $Le = 1.5$ and $M^* = 1.5$.

function at the onset of the subcritical convective solutions are predicted by the parallel flow approximation. Here, $R_{TC}^{sub1} = R_{TC}^{sub2}$ and $|\Psi_{0cr}^1| = \Psi_{0cr}^2$ in the absence of lateral heating ($a = 0$). The increase of a leads to a decrease/(increase) of R_{TC}^{sub1} and $|\Psi_{0cr}^1|$/(R_{TC}^{sub2} and $|\Psi_{0cr}^2|$). More precisely, when the value of a increases from 0 to 1, R_{TC}^{sub1}/(R_{TC}^{sub2}) decreases/(increases) from 12.44/(12.44) to 5.96/(50.13) and $|\Psi_{0cr}^1|$/(Ψ_{0cr}^2) passes from 0.77/(0.77) to 0.67/(2.01). Therefore the lateral heating promotes/(delays) the onset of the sub-critical convection corresponding to the CF/(CCF).

5.3. Combined effect of a and R_T

The influence of lateral heating on the fluid flow and heat and mass transfer characteristics is analyzed for the cases $(Le,\ M^*) = (3, 2)$ and (1.5, 1.5), corresponding to a single subcritical bifurcation and two subcritical bifurcations, respectively. Fig. 10a–c shows the variations of Ψ_0, Nu and Sh with R_T for $(Le,\ M^*) = (3, 2)$ and various values of a. For $a = 0$, only supercritical convection exists, which leads to two symmetrical convective solutions starting from the rest state ($\Psi_0 = 0$, $Nu = 1$ and $Sh = 2$) at $R_T = R_{TC}^{sup} = 4$. By increasing a, a subcritical bifurcation is triggered earlier than the supercritical one at a given value of $R_T = R_{TC}^{sub} < R_{TC}^{sup}$. In the range $R_{TC}^{sub} < R_T < R_{TC}^{sup}$, two convective solutions rotating in the same direction are obtained, while for $R_T > R_{TC}^{sup}$, the flow corresponding to one of these two solutions changes its rotation direction. The symmetry displayed by the curve of Ψ_0 in the case of $a = 0$ is destroyed in the presence of lateral heating ($a > 0$). Lateral heating enhances the flow intensity of the CF solution and the corresponding Nusselt number; this tendency is reversed in the case of counter-clockwise flow. The variations of Sh with R_T, presented in Fig. 10c, are somewhat surprising since Sh remains insensitive to the variation of a and to the flow direction.

The case of $(Le, M^*) = (1.5, 1.5)$ is illustrated in Fig. 11a–c. For a given value of a, this combination of

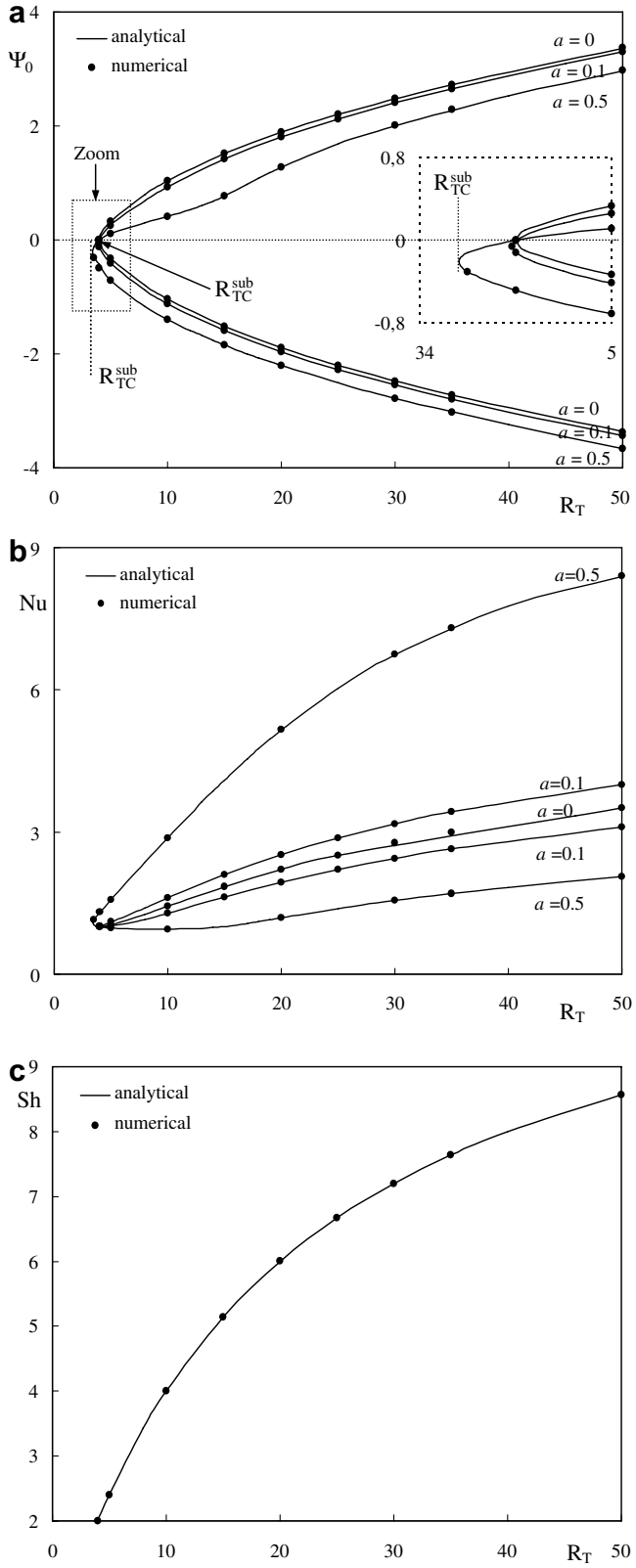

Fig. 10. Variations with R_T of (a) Ψ_0, (b) *Nu* and (c) *Sh* for $Le = 3$, $M^* = 2$ and $a = 0$, 0.1 and 0.5.

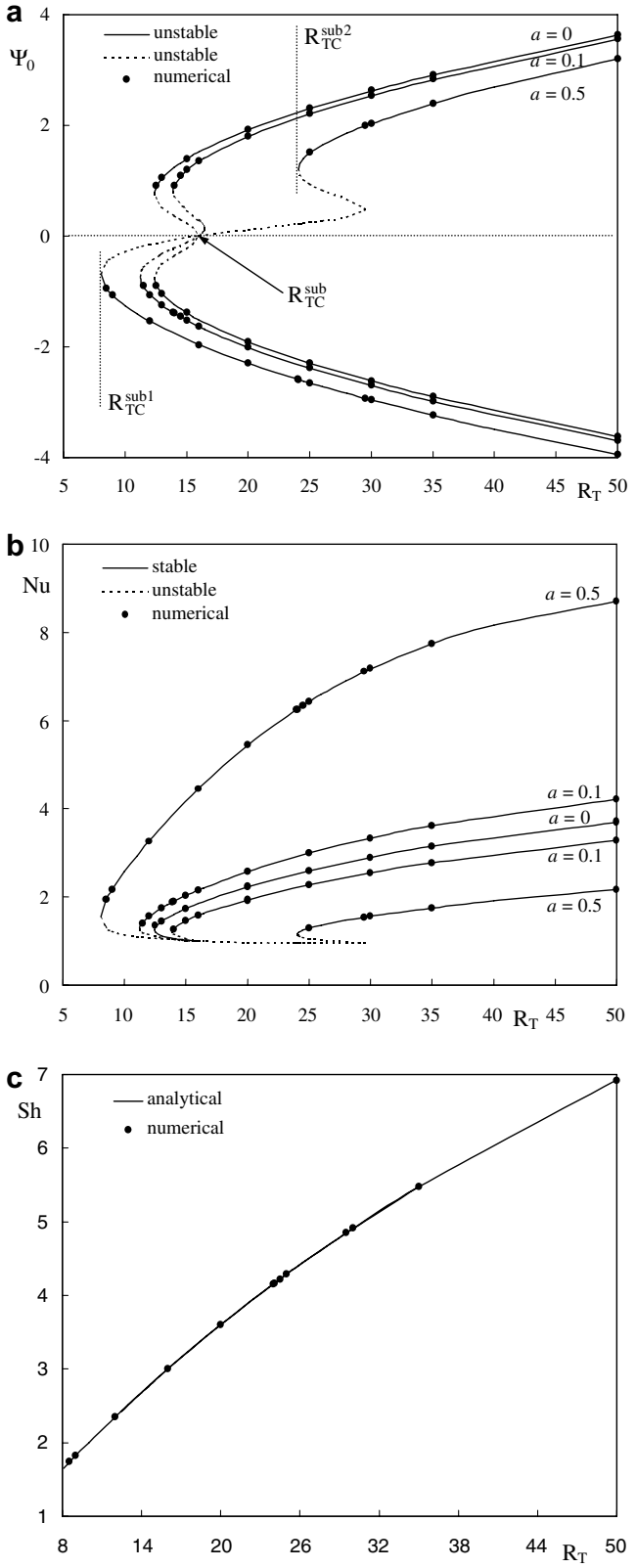

Fig. 11. Variations with R_T of (a) Ψ_0, (b) *Nu* and (c) *Sh* for $Le = 1.5$, $M^* = 1.5$ and $a = 0$, 0.1 and 0.5.

(Le, M^*) is characterized by the presence of two subcritical bifurcations corresponding to two critical values of the Rayleigh number: R_{TC}^{sub1} (corresponding to the onset of the subcritical CF) and R_{TC}^{sub2} (corresponding to the onset of

the subcritical CCF). For $a = 0$, the two subcritical flows start at the same critical value of $R_T(R_{TC}^{sub1} = R_{TC}^{sub2} = 12.44)$ and the presence of the lateral heating precipitates/(retards) the appearance of the CF/(CCF). In the case of the stable solutions (represented by continuous lines), the lateral heating enhances/(reduces) the intensity and the Nusselt number resulting from the CF/(CCF). However, once again, the Sherwood number is independent of the parameter a and of the flow direction.

5.4. Effect of a on the multiplicity of solutions

The effect of lateral heating on the multiplicity of solutions is examined for a combination of $(R_T, M^*, Le) = (15, 1.5, 1.5)$, leading to four different solutions in the absence of lateral heating. The variations of Ψ_0 with a, presented in Fig. 12a, show that four convective solutions are possible for small values of a, characterized by two CF (with intensities of Ψ_{0C}^1 and Ψ_{0C}^2) and two CCF solutions (with intensities of Ψ_{0T}^1 and Ψ_{0T}^2). By increasing a from 0 (for which $\Psi_{0C}^1 = -\Psi_{0T}^1$ and $\Psi_{0C}^2 = -\Psi_{0T}^2$) to 1, the intensity Ψ_{0T}^1 of the stable branch of the CCF decreases while the intensity Ψ_{0T}^2 of the unstable branch (probably not a physical solution) increases. Above the critical value $a_{cr} \approx 0.17$, these two CCF solutions become unstable due to lateral heating, and revert their flow circulation to CF. The lateral heating induces an increase of $|\Psi_{0C}^1|$ and a decrease of $|\Psi_{0C}^2|$ (probably not a physical solution). In Fig. 12b, which shows the variations of Nu induced by the different solutions with a, the greatest heat transfer is engendered by the stable CF. Sh curves are not presented here since the obtained Sh values were constant ($Sh = 2.84$) and independent of a.

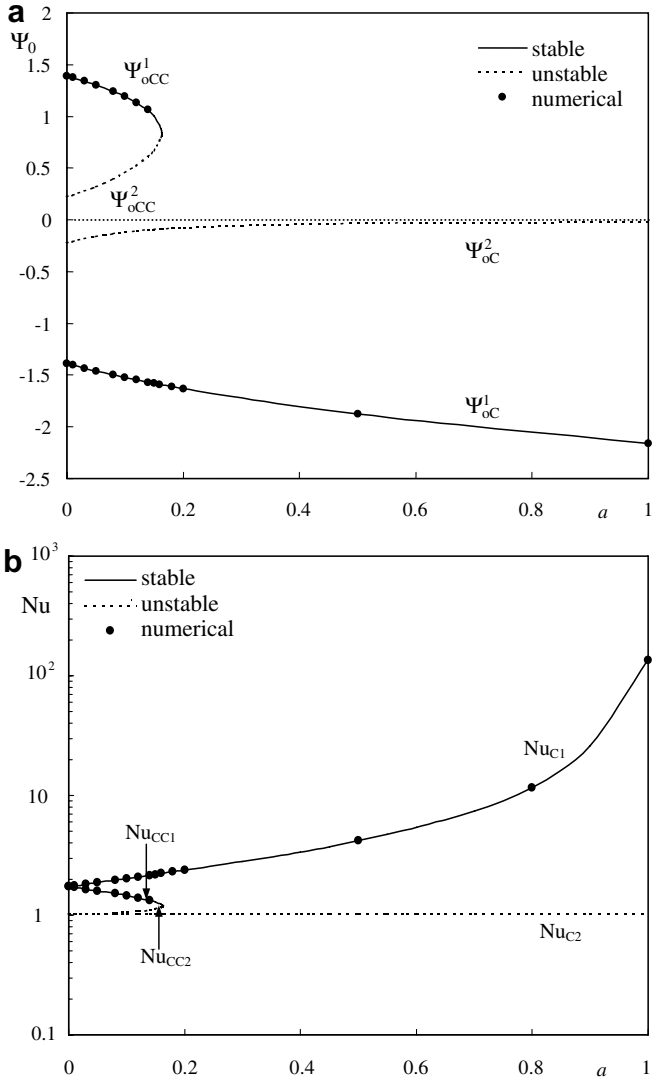

Fig. 12. Variations with a of (a) Ψ_0 and (b) Nu for $R_T = 15$, $Le = 1.5$ and $M^* = 1.5$.

6. Conclusions

Double diffusive natural convection in a horizontal Darcy porous layer subject to uniform fluxes of heat and mass was studied analytically (parallel flow approximation) and numerically in the presence of the Soret effect. Attention was focused on the case where the Soret separation ratio $\varphi = -MN = -1$, for which the effect of lateral heating was balanced by the Soret effect. For this case, the rest state was a solution of the problem. The critical conditions corresponding to the onset of subcritical and supercritical bifurcations for the parallel flow solution were determined analytically. The plane Le–M^* (i.e., $M^* = 1/M$) could be divided into five regions with specific behaviors. Depending on the considered region, up to two subcritical bifurcations were possible with or without supercritical bifurcation. When both subcritical bifurcations existed, at least one of them (corresponding to clockwise flow) started earlier than the supercritical bifurcation. Also, the existence of one region characterized by negative values of M^*, where a parallel flow solution was not possible, was delineated. The surprising finding of the study was the insensitivity of the Sherwood number vis-à-vis the lateral heating and the multiplicity of solutions in spite of the fact that the latter had a considerable effect on the flow intensity and Nusselt number.

References

[1] J.K. Platten, The Soret effect: a review of recent experimental results, J. Appl. Mech. 73 (2006) 5–15.
[2] R. Rosanne, M. Paszkuta, E. Tevissen, P.M. Adler, Thermodiffusion in a compact clay, J. Colloid Interf. Sci. 267 (2003) 194–203.
[3] A. Mansour, A. Amahmid, M. Hasnaoui, M. Bourich, Numerical study of the multiplicity of solutions induced by thermosolutal convection in a square porous cavity heated from below and submitted to horizontal concentration gradient in the presence of Soret effect, Numerical Heat Transfer, Part A 49 (2006) 69–94.
[4] L.B. Benano-Melly, J.P. Caltagirone, B. Faissat, F. Montel, P. Costeseque, Modeling Soret coefficient measurement experiments in porous media considering thermal and solutal convection, Int. J. Heat Mass Transfer 44 (2001) 1285–1297.

[5] M. Ouriemi, P. Vasseur, A. Bahloul, Natural convection of a binary mixture confined in a slightly inclined tall enclosure, Int. Commun. Heat Mass Transfer 32 (2005) 770–778.
[6] R. Bennacer, A. Mahidjiba, P. Vasseur, H. Beji, R. Duval, The Soret effect on convection in a horizontal porous domain under cross temperature and concentration gradients, Int. J. Numerical Methods Heat Transfer Fluid Flow 13 (2003) 199–215.
[7] M. Marcoux, M.C. Charrier-Mojtabi, A. Bergeon, Naissance de la thermogravitation dans un mélange binaire imprégnant un milieu poreux, Entropie 214 (1998) 31–36.
[8] F. Joly, P. Vasseur, G. Labrosse, Soret instability in a vertical Brinkman porous enclosure, Numerical Heat Transfer, Part A 39 (2001) 339–359.
[9] I. Rehberg, G. Ahlers, Experimental observation of a codimension-two bifurcation in a binary fluid mixture, Phys. Rev. Lett. 55 (1985) 500–503.
[10] S.M. Alex, P.R. Patil, Effect of variable gravity field on Soret driven thermosolutal convection in a porous medium, Int. Commun. Heat Mass Transfer 28 (2001) 509–518.
[11] O. Sovran, M.C. Charrier-Mojtabi, A. Mojtabi, Naissance de la convection thermo-solutale en couche poreuse infinie avec effet Soret, C. R. Acad. Sci. Paris 329 (2001) 287–293.
[12] C. Karcher, U. Müller, Bénard convection in binary mixture with a nonlinear density–temperature relation, Phys. Rev. E 49 (1994) 4031–4043.
[13] A. Bahloul, N. Boutana, P. Vasseur, Double-diffusive and Soret-induced convection in a shallow horizontal porous layer, J. Fluid Mech. 491 (2003) 325–352.
[14] M. Bourich, M. Hasnaoui, M. Mamou, A. Amahmid, Soret effect inducing subcritical and Hopf bifurcations in a shallow enclosure filled with a clear binary fluid or a saturated porous medium: a comparative study, Phys. Fluids 16 (2004) 551–568.
[15] M. Bourich, M. Hasnaoui, A. Amahmid, M. Mamou, Soret convection in a shallow porous cavity submitted to uniform fluxes of heat and mass, Int. Commun. Heat Mass Transfer 31 (2004) 773–782.
[16] A. Ryskin, H.W. Müller, H. Pleiner, Thermal convection in binary fluid mixtures with a weak concentration diffusivity, but strong solutal buoyancy forces, Phys. Rev. E 67 (2003) 1–8.
[17] R. Delahaye, A. Bahloul, P. Vasseur, Influence of the Soret effect on convection in a binary fluid layer with a free upper surface, Int. Commun. Heat Mass Transfer 29 (2002) 433–442.
[18] A. Mahidjiba, R. Bennacer, P. Vasseur, Flows in a fluid layer induced by the combined action of a shear stress and the Soret effect, Int. J. Heat Mass Transfer 49 (2005) 1403–1411.
[19] M. Ouriemi, P. Vasseur, A. Bahloul, Natural convection of a binary fluid in a slightly inclined shallow cavity, Numerical Heat Transfer, Part A 48 (2005) 547–565.
[20] M.C. Charrier-Mojtabi, Y.P. Razi, K. Maliwan, A. Mojtabi, Influence of vibration on Soret-driven convection in porous media, Numerical Heat Transfer, Part A 46 (2004) 981–993.
[21] M. Bourich, A. Amahmid, M. Hasnaoui, Double diffusive convection in a porous enclosure submitted to cross gradients of temperature and concentration, Energy Conver. Manage. 45 (2004) 1655–1670.
[22] O.V. Trevisan, A. Bejan, Natural convection with combined heat and mass transfer buoyancy effects in porous medium, Int. J. Heat Mass Transfer 29 (1985) 1597–1611.